Automated Step Change Detection in Real-World PMU Data Addressing Practical Implications

Mohammad MansourLakouraj, *Member, IEEE*, Chetan Mishra, *Member, IEEE*, Luigi Vanfretti, *Senior Member, IEEE*, Jaime De La Ree Jr., Kevin D. Jones, and Hanif Livani, *Senior Member, IEEE*

***Abstract*—This paper introduces a fully automated and unsupervised technique for detecting step changes in synchrophasor measurements, without prior knowledge or learning data features, and without applying the complex task of baselining and parameter tuning. Step changes in synchrophasor measurements occur due to shunt switching, controller set point changes, etc. With increasing grid oscillations from inverter-based resources (IBRs), step changes are vital for tracking grid response and anticipating IBR controller-related oscillations. This study identifies step changes through a *nonorthogonal* discrete wavelet transform that relies on smoothed gradient estimation. A non-linear filter based on a multiscale point-wise product of wavelet coefficients is proposed, which takes advantage of the broadband feature of step changes within the space of wavelet coefficients. This filter also eliminates unwanted signal elements, thus decreasing the occurrence of false positives. Finally, through the statistical characterization of multi-scale products, we use an adaptive multiscale dependent threshold for detecting steps amidst real-world measurement noise and grid oscillations. Our studies indicate the effectiveness of our method in detecting step changes in synchrophasor data, supported by showcasing real-world case studies and discussing practical applications. Our method also significantly outperforms the relevant baseline detection methods by measuring Accuracy, F1 Score, and Precision under both ambient (noise) and step change conditions.**

***Index Terms*—step detection applications, PMU, nonorthogonal wavelets, non-linear filtering, adaptive thresholding, real-world problems.**

I. Introduction

Phasor measurement units (PMUs) deliver precise, time-synchronized data from various locations, enabling utilities to enhance their comprehension of grid behavior and their capacity to detect system issues [1]. PMUs are particularly useful for managing oscillations from inverter-based resources and conventional power plants [2]. Using PMUs to monitor such kind of plant interactions enables new control schemes or parameter adjustments, preventing oscillations [3]. In addition, a potential problem that could arise due to weakened power grid conditions is voltage stability. To address this problem, PMU data-driven techniques use a Thévenin equivalent [4] of the grid as seen through a load bus to assess voltage stability. A significant challenge in addressing these monitoring issues practically is the simultaneous interaction of numerous components with the grid. Therefore, it is necessary to choose the suitable data window, where the relevant grid dynamics are dominant for the problem being addressed.

In the context of monitoring deteriorating grid conditions, it is possible to address this by identifying instances where there are *step changes* in key variables like voltage magnitude and active/reactive power of a power plant. In [5], a very specific PV plant response due to a topological change near inverter-based resources was analyzed by examining step changes in PMU data; however, this step-like pattern has been manually identified. Other applications that can be aided by step detection and time localization include inertia estimation [6] and generator model validation [7]. Step changes in the measured signal are also used in system identification with probing-based methods to find bus sensitivities or impedance equivalents, which are used for the stability analysis of distributed energy resources (DERs) and the control of DERs based on inverters [8]. In addition to the applications mentioned above, step detection also plays an important role in instrumentation development. The National Metrology Institute (NMI) have advanced PMU calibration systems [9], [10] to better align with IEEE Std. requirements. Attention has been paid to dynamic tests [11] and the definition of accuracy limits for calibrators. For tests involving magnitude and phase steps, detecting steps and knowing the *time of step change* is crucial [12].

PMU-based monitoring and detection applications exploit *signal processing* techniques such as the Fourier transform, wavelet, etc., as effective means of extracting and analyzing relevant features of the power grid's dynamics that are present in the ambient data [13], [14]. Regardless of the specific signal processing method used for this purpose, threshold values are needed to determine if the system performance has deteriorated. The typical method involves using a "predefined" threshold, which depends on ambient data to set confidence levels for identifying large sudden changes [15]. Learning-based approaches require adjusting various parameters to set a reliable threshold for identifying events using training data sets [16], [17]. Implementing these strategies in practice is difficult due to the need for significant historical data and prior knowledge to set thresholds. They are primarily designed to detect events that create significant variations in measured

M. MansourLakouraj and H. Livani are with the Department of Electrical and Biomedical Engineering, University of Nevada, Reno, Reno, NV 89557, USA. C. Mishra, J. De La Ree Jr., and K. D. Jones are with Dominion Energy, Richmond, VA, US. L. Vanfretti is with the ECSE Department, Rensselaer Polytechnic Institute, Troy, NY. Emails: m.mansour349@gmail.com, hlivani@unr.edu, and luigi.vanfretti@gmail.com

This work is supported by the U.S. National Science Foundation under Grant ECCS-2033927.

data (e.g., voltage and frequency), such as outages and trips. However, they may not be effective at detecting certain changes of interest for analysis, such as steps in signals under ambient conditions. As power system dynamics evolve with the integration of renewables [5], data centers, and emerging technologies, frequent updates and thorough baselining are essential to adapt to changing grid dynamics. Furthermore, the time location of abrupt changes, required to analyze dynamic responses [18], along with reduced sensitivity to noise and oscillations—which helps avoid false alarms in practice—are key features addressed in this study.

To resolve these needs, we employ a gradient estimation-based *non-orthogonal* discrete wavelet transformation (DWT) as described in [19], along with product-based filtering on adjacent wavelet scales [20], [21], as viable solutions to enhance step/edge detection in PMU data. This class of wavelets is also referred to as Mallat and Zhong (MZ)-DWT. The proposed non-orthogonal wavelet demonstrates a significantly better characterization of abrupt changes compared to the widely used Daubechies orthogonal wavelet [15], as evidenced by our preliminary analysis of the step detection [see Section D of Section 3 in [22]].

In this paper, we employ MZ-DWT and a nonlinear filtering process to establish a robust, adaptive threshold based on the statistical features of scales, relying solely on available monitored data *without* requiring historical data or a training process for *different applications*. In summary, the contributions of this work are listed as follows:

- A three-stage step detection framework, consisting of nonorthogonal wavelet transformation, non-linear product-based filtering, and inter-scale thresholding, is proposed to detect step changes in PMU data, applicable to both ambient and transient (event) conditions.
- The proposed method exploits nonorthogonal gradient estimation-based wavelet theory, which is applied for accurate detection of edges/steps with time localization under noise and natural oscillations. This nonorthogonal transformation provides better signatures of the step changes across multiscales in the wavelet domain for enhanced detection purposes.
- A nonlinear filter derived from the pointwise product of scales generates a detection signal characterized by reduced noise interference and *distinct maxima* linked to step changes in the original data, aiding in thresholding.
- An adaptive threshold is proposed by statistically examining multiscale dependencies within nonorthogonal wavelet transforms of PMU signals. This method improves detection accuracy and reduces false alarms by studying noise characteristics across adjacent *wavelet scales* in each monitored window of data, ensuring high adaptivity to the ongoing dynamical changes in the system.
- The method is a fully unsupervised, automated technique that requires no historical data or training, no parameter tuning, and no baselining, which are usually big challenges in real-world utility settings. The proposed method's significance is further examined for real-world uses, such as characterizing signal patterns, pinpointing change origins, and utilizing time localization to select suitable data windows.

In the following section, the proposed methodology is given (Section II). The numerical studies are presented in Section III. In Section IV, further applications and discussions are shown, and Section V provides comparisons with other methods. Finally, we conclude the paper in Section VI.

II. Step Detection Methodology

A. Nonorthogonal Discrete Wavelet Transform

The wavelet transform, when applied to a function $g(x)$ at a designated scale s and specific location x, is represented as $W_s g = g(x) * \psi_s(x)$, where the symbol $*$ denotes convolution and $\psi_s(x) = \psi\left(\frac{x}{s}\right)$ defines a re-scaled function.

The signal's instantaneous characteristics can be highlighted by designing the wavelet transform as a multiscale edge detector. Let $\theta(x)$ be a differentiable function whose integral equals one and reaches zero as $x \to \infty$, and let $\psi(x) = \frac{d\theta(x)}{dx}$, then the wavelet transform $W_s g(x)$ expressed as:

$$W_s g(x) = g * \left(s\frac{d\theta_s}{dx}\right)(x) = s\frac{d}{dx}(g * \theta_s)(x). \tag{1}$$

In this formulation, the wavelet transform $W_s g(x)$ constitutes the derivative of $g(x)$, further smoothed by $\theta_s(x)$. Particularly, when using a *Gaussian* function for $\theta(x)$, the identification of local extrema within $W_s g(x)$ becomes similar to the effective *Canny edge detection* algorithm [23], [24].

To enhance numerical performance, we confine the scale s to be along the dyadic sequence $(2^j)_{j\in\mathbb{Z}}$. Therefore, the dilation of $\psi(x)$ by 2^j is represented as $\psi_j(x) = \frac{\psi\left(\frac{x}{2^j}\right)}{2^j}$. The discrete transform of $g(x)$ at the dyadic scale 2^j and specific location x is defined as:

$$W_j g = g(x) * \psi_j(x). \tag{2}$$

It should be noted that by requiring two strictly positive constants C_1 and C_2 provided that $C_1 \leq \sum_{j=-\infty}^{+\infty} |\hat{\psi}(2^j\omega)|^2 \leq C_2 \quad , \forall \omega \in \mathbb{R}$, we ensure that the entire frequency spectrum is covered by the dilations of $\hat{\psi}(\omega)$ by 2^j, where $j \in \mathbb{Z}$. Consequently, $\hat{g}(\omega)$ and thus $g(x)$ can be reconstructed from its dyadic wavelet transform. The original function $g(x)$ is reconstructable from its discrete wavelet coefficients via

$$g(x) = \sum_{j=-\infty}^{\infty} W_j g * \gamma_j(x) \tag{3}$$

where $\gamma(x)$ indicates any reconstructing wavelet whose Fourier transform satisfies

$$\sum_{j=-\infty}^{\infty} \hat{\psi}(2^j\omega)\hat{\gamma}(2^j\omega) = 1. \tag{4}$$

In this study, the wavelet $\psi(x)$ is designed as a quadratic spline function that resembles the first derivative of a Gaussian.

Consequently, the proposed wavelet transform works similarly to an edge detector. The following subsections will detail the computation of this wavelet and the discrete decomposition of this specific wavelet transformation.

1) Defining Quadratic Spline Wavelets: This section defines a class of wavelets suitable for the efficient implementation of discrete algorithms [19]. The Fourier transform of the smoothing function $\phi(x)$ can be expressed as an infinite product[1]

$$\hat{\phi}(\omega) = e^{-i\omega} \prod_{p=1}^{+\infty} G(2^{-p}\omega) \tag{5}$$

where $G(\omega)$ is a 2π periodic function satisfying

$$|G(\omega)|^2 + |G(\omega + \pi)|^2 \leq 1. \tag{6}$$

In the above, $|G(0)|$ is equal to 1, and w represents the sampling shift, which is adjusted so that $\phi(x)$ is symmetric around 0. Expression (5) indicates that

$$\hat{\phi}(2\omega) = e^{-i\omega} G(\omega)\hat{\phi}(\omega). \tag{7}$$

A wavelet $\psi(x)$ is defined with its Fourier transform $\hat{\psi}(\omega)$ represented by

$$\hat{\psi}(\omega) = e^{-i\omega w} H(\omega)\hat{\phi}(\omega) \tag{8}$$

where $H(\omega)$ is a function with a period of 2π, and it is proven that $\hat{\psi}(\omega)$, $\hat{\gamma}(\omega)$, and $\hat{\phi}(\omega)$ satisfies

$$\hat{\psi}(2\omega)\hat{\gamma}(2\omega) = |\hat{\phi}(\omega)|^2 - |\hat{\phi}(2\omega)|^2. \tag{9}$$

It is assumed that $\hat{\gamma}(\omega)$ can be expressed as

$$\hat{\gamma}(2\omega) = e^{iw\omega} Z(\omega)\hat{\phi}(\omega) \tag{10}$$

where $Z(\omega)$ represents a function that is 2π periodic. By substituting (7) and (10) into (9), we have

$$H(\omega)Z(\omega) + |G(\omega)|^2 = 1. \tag{11}$$

Equation (11) provides a sufficient condition for defining $Z(\omega)$ such that $\hat{\gamma}(\omega)$ corresponds to the Fourier transform of a reconstructing wavelet, thereby satisfying (4).

Our goal is to define a wavelet $\psi(x)$ as the first-order derivative of a smoothing function $\theta(x)$, which is antisymmetric and maximizes regularity. Consequently, $\hat{\psi}(\omega)$ should exhibit a first-order zero at $\omega = 0$. Given that $|\hat{\phi}(0)| = 1$, it follows from equation (8) that $G(\omega)$ must have a first-order zero at $\omega = 0$. The set of 2π-periodic functions $G(\omega)$, $H(\omega)$, and $Z(\omega)$ that meet the defined constraints given by:

$$G(\omega) = e^{i\omega/2}(\cos(\omega/2))^3, \tag{12}$$

$$H(\omega) = 4ie^{i\omega/2}\sin(\omega/2), \tag{13}$$

$$Z(\omega) = \frac{1 - |G(\omega)|^2}{H(\omega)}. \tag{14}$$

The periodic functions $G(\omega)$, $H(\omega)$, and $Z(\omega)$ correspond to the *transfer functions of discrete filters* with finite impulse responses. These filters play a crucial role in the computation of fast wavelet transforms, as described in the next section.

Based on equations (5) and (8), it is inferred

$$\hat{\phi}(\omega) = \left(\frac{\sin(\omega/2)}{\omega/2}\right)^3, \tag{15}$$

$$\hat{\psi}(\omega) = i\omega\left(\frac{\sin(\omega/4)}{\omega/4}\right)^4. \tag{16}$$

To ensure that the wavelet $\psi(x)$ is antisymmetric with respect to 0 and $\phi(x)$ is symmetric with respect to 0, the shifting constant w of (7) is set to $1/2$. Equation (16) ensures that $\psi(x)$ is a quadratic spline.

2) Algorithm for Computing Discrete Transforms: This section presents a discrete wavelet transformation method to analyze the signal at different scales. We define wavelet function $\psi(x)$ by three computed filters: H, G, and Z.

H_p, G_p, and Z_p are discrete filters formed by inserting $2^p - 1$ zeros among the coefficients of H, G, and Z. Thus, the transfer functions for these particular filters are represented as $H(2^p\omega)$, $G(2^p\omega)$, and $Z(2^p\omega)$.

Algorithm 1 performs the wavelet transform on discrete PMU signal $S_1^d g$. At each level 2^j, it splits $S_{2^j}^d g$ into $S_{2^{j+1}}^d g$ and $W_{2^{j+1}}^d g$.

Algorithm 1: Discrete Wavelet Transformation

Data: PMU signal $S_1^d g$, scale J, discrete filters H_j and G_j, scaling constants ς_j.
Result: Wavelet coefficients $W_j^d g$ and scale coefficients $S_j^d g$ for each scale j.
Initialization; $j = 0$;
while $j < J$ **do**
- $\mathrm{W}_{2^{j+1}}^d g = \frac{1}{\varsigma_j} \mathrm{S}_{2^j}^d g * H_j$;
- $\mathrm{S}_{2^{j+1}}^d g = \mathrm{S}_{2^j}^d g * G_j$;
- $j = j + 1$;

end

For precise Lipschitz exponent estimations each dyadic increment 2^j, the sample values from $S_{2^j}^d g * H_j$ are adjusted by ς_j to correct discretization effects. This ensures wavelet modulus peaks at step edges are consistent across scales, unlike in a continuous paradigm. The ς_j factors mitigate discrete scenario discrepancies, with values for filters in [19].

B. Multiscale Nonlinear Filtering

The signal's behavior in the wavelet domain depends on its local smoothness, quantifiable by Lipshitz exponents. $g(x)$ is Lipshitz continuous at x_0 for $0 \leq \alpha \leq 1$ if a constant K_0 exists such that near x_0:

$$|g(x) - g(x_0)| \leq K_0|x - x_0|^\alpha. \tag{17}$$

The term *Lipshitz regularity* is assigned to the maximal limit for all α satisfying (17). Equation (18) describes the correlation between α and the amplitude of the wavelet as shown in [26]:

$$|W_j g| \leq K_1(2^j)^\alpha \tag{18}$$

where K_1 indicates a predefined constant. A step discontinuity has a Lipshitz regularity of zero, generalizable to negative

[1]As shown in [25], the conditions in (6) guarantee that (5) defines a smoothing function $\phi(x)$ that belongs to $L^2(\mathbb{R})$.

values for more extreme singularities, such as white noise. White noise has a Lipshitz regularity of -0.5 [27]. As deduced from Equation (18), for signal singularities with Lipshitz regularities $\alpha > 0$, the wavelet transform magnitudes increase or remain constant as the scale 2^j increases. Conversely, due to white noise's negative Lipshitz regularity, the transform magnitudes diminish quickly across scales.

Implementing MZ-DWT reveals that signal singularities evolve across scales with noticeable peaks, while noise rapidly diminishes along these scales. Consequently, multiplying the wavelet transforms at adjacent scales can be viewed as a method to amplify edge structures while reducing noise. This property motivates us to discuss the multiscale nonlinear filtering method.

Multiscale point-wise products have been suggested to enhance peaks associated with steps and suppress noise [20]. Therefore, a practical application necessitates multiplication at merely two consecutive scales as:

$$P_j g = W_j g \cdot W_{j+1} g. \tag{19}$$

As a result, in the (noisy) measured signal $g = f + \epsilon$, f's salient features (step changes) become more prominent in the multiscale-based filtered signal $P_{j,f}$ as compared to single scale transformation $W_j g$. Thus, $P_j g$ is chosen as our *detection signal* to set the threshold because it further diminishes the impact of noise and gives *very distinct local maxima associated with step changes*, potentially improving the step detection process.

C. Adaptive Multiscale Thresholding

This section introduces *adaptive multiscale-based thresholding* using the inter-scale dependencies of wavelets on the detection signal $P_j g$ [24]. Considering that the wavelet transform operates *linearly*, the decomposition of a noisy signal $g = f + \epsilon$ through the discrete wavelet transform is expressed as:

$$W_j g = W_j f + W_j \epsilon \tag{20}$$

where $W_j f$ represents the wavelet transform of the signal f without noise, and $W_j \epsilon$ the transform of the additive noise ϵ.

An adaptive threshold applied to $P_j g$ can differentiate large step peaks (maxima) from smaller noise peaks, automating step detection. To this end, assuming the presence of solely noise ϵ in the input, the multiscale products function, $P_j \epsilon = W_j \epsilon \cdot W_{j+1} \epsilon$, arises, where $W_j \epsilon$ and $W_{j+1} \epsilon$ are two noise components at different scales. These two components are jointly Gaussian with standard deviations for these are σ_j and σ_{j+1}, respectively, coupled with a correlation coefficient of

$$\rho_{j,j+1} = \frac{\operatorname{cov}(W_j \epsilon, W_{j+1} \epsilon)}{\sigma_j \sigma_{j+1}}. \tag{21}$$

The standard deviation for the products function $P_j \epsilon$ is given by

$$\tau = \sigma_j \sigma_{j+1} \cdot \sqrt{1 + 2\rho_{j,j+1}^2}. \tag{22}$$

In practice, the input is composed of a mixture of noise and the actual signal, with noise considerably influencing the response (depending on its level). However, by setting a threshold $t_d = c \cdot \tau$, where $c > 5$, essential edge details are preserved and noise is suppressed [28].

Inspired by these statistical characteristics, we use t_d as our threshold, and we set $c = 6$ based on our experiments working with real-world data. Moreover, the correlation of scales is quantified in [21] under Gaussian noise and is used in our calculations. For example, the correlation between scales 3 and 4 is 0.68. Regarding the calculation of variance on different scales, the median absolute deviation (MAD) operator is used as $\frac{\text{MAD}(W_j g)}{0.6745}$ to calculate the variance on each transformed scale [29].

It is worth mentioning that assuming noise with Gaussian characteristics is realistic based on real-world statistical analysis, especially for magnitude signals such as those used in this study [30], [31]. However, to verify this on the basis of the available data set, Q-Q plots and the autocorrelation function can be used to test the Gaussianity of the noise. If it deviates *considerably*, a whitening process may be applied to the data. However, this is beyond the scope of our current study.

D. Proposed Framework for Power System Applications

The proposed three-stage framework for step detection leverages previous theory and formulations to: 1) apply a non-orthogonal wavelet transform using smoothed gradient estimates, 2) use nonlinear filtering through multiplying adjacent wavelet scales to extract a signal with local peaks indicating steps, and 3) set an adaptive threshold by analyzing the statistical features of the scales and their products to distinguish noise from step patterns.

A detailed flowchart of the proposed method and its potential application for energy utilities is depicted in Fig. 1. This figure additionally delineates the computations executed at each stage of the method and correlates them with the previously discussed equations and Algorithm 1. Outlined below is the sequence of essential steps we employ for each incoming data window, allowing us to dynamically and efficiently set the multiscale threshold and adjust to the system's continuous changes:

- Stage 1: Wavelet Nonorthogonal Transformations
  - Defining the wavelet filters with the computed transfer functions.
  - Execute *Algorithm 1* to determine scales.
- Stage 2: Non-linear Multiscale Filtering
  - Select adjacent non-orthogonal scales.
  - Perform a multi-point product of multi scales to suppress noise and extract step change signatures.
- Stage 3: Adaptive Multiscale Threshold Computation
  - Compute the correlation of selected wavelet multi scales $\rho_{(j,j+1)}$ (see Equation (21)).
  - Compute noise variance on each scale.
  - Compute the standard deviation of the jointly Gaussian function describing the features of multi (adjacent) scales (scales $j, j+1$) (see Equation (22)).

– Calculate the multiscale threshold t_d for the chosen window data with $c > 5$, which ensures the reduction of the probability of false alarms and minimization of noise impact. The threshold is finally defined as $t_d = c \cdot \tau = c \cdot \sigma_j \sigma_{(j+1)} \sqrt{1 + 2\rho^2_{(j,j+1)}}$.

The parameters of the threshold (t_d), such as the correlation and variance of adjacent scales $(j, j+1)$, are computed and updated in each window and are not fixed values for the entire dataset. Our method's distinction lies in its dynamic multiscale analysis of each data window, utilizing continuous statistical evaluations to discern noise and step characteristics, thereby enhancing its adaptability to system changes.

In the subsequent sections, we will showcase the applications and advantages of the proposed method in detail, with numerous case studies and comprehensive comparisons with the relevant technologies.

III. Numerical Studies of Real-World Scenarios

In this section, we demonstrate the proposed method effectiveness using real-world PMU data from Dominion Energy. The synchrophasor data, reported at a rate of 30 phasors per second, were obtained from digital fault recorders at different substations. We focus on the positive sequence voltage magnitude data to evaluate our method.

A. Case 1: Characterizing Different Edges

In this case, voltage data recorded for two minutes was obtained from a 230-kV substation. This data includes one step, sharp spikes as well as noise (see plot (a) in Fig. 2). Here, we aim to demonstrate that the proposed approach can differentiate the step characteristics from other patterns. The MZ-DWT is applied and four transformations are shown in plots (b)-(e) in Fig. 2. The first scale (see Fig. 2(b))includes high-frequency variations, and each large spike in (a) is represented as two consecutive spikes moving in opposite directions in (b). The characteristic features of spikes and noise become less pronounced in larger scales, (see Fig. 2(d) and (e)) by increasing the smoothness in the nonorthogonal transformation. On the other hand, when the step moves upward, larger scale transformations (especially scales 3 and 4, (d) and (e) in Fig. 2, respectively) clearly show this step with a *distinctive local maxima*. Thanks to the nonorthogonal transformation, the time frame length and the location of changes are preserved, which is useful information for selecting the appropriate window of data for further analysis. This is in sharp contrast to orthogonal transformations, which change the data length at each scale of the wavelet transform, thereby losing the timing of the changes.

To enhance step peaks and reduce noise, we apply nonlinear filtering using a multiscale point-wise product. We use multiscale nonlinear filtering at scales 3 and 4 for step detection, which suppresses noise and sharpens step peaks. Experiments show more false extrema with other scales, so scales 3 and 4 are used for all following cases.

Figure 3 shows the results of the proposed nonlinear filtering, with distinct peaks and significantly suppressed noise. It is important to observe that the peaks are mainly positive due to the even count of products and the uniform direction of extrema across various scales. However, peaks from isolated spikes between 09:09:00 and 09:09:45 in the original PMU data are reduced due to higher scale smoothing. This enhances thresholding performance, distinguishing step-related peaks from other suppressed maxima. Identifying narrow edges and spikes can be aided by smaller scales, but our focus is on automating step detection for the utilities needs.

B. Case 2: Controllers' Interaction

This section examines the response of an OLTC at a substation near a 69 kV solar power plant. As shown in [13], *oscillations* at solar power plants are significant during morning and late afternoon, under specific controller control modes. In this substation, due to the OLTC's proximity to the solar site, its increased responsiveness adversely affects its lifetime and maintenance costs. Two scenarios are considered below.

The first scenario considers the voltage magnitude measurements are shown in Fig. 4(a), where an oscillation is apparent. Note that it is known that the tap position changes twice during this voltage period. These changes create two edges on the voltage data recorded by the PMU, which can *hardly* be seen in Fig. 4. All MZ-DWT results shown in Fig. 4 (b)-(e) indicate the characterized signature (distinctive peaks) of these two-step changes hidden under severe oscillation. The multiscale filtered data and threshold can effectively detect these two peaks exactly, as shown in Fig. 5.

In the second scenario, the voltage data is recorded in the morning at the same substation and is shown in Fig. 6(a). Again, when voltage oscillations occur, the number of tap changes increases, resulting in steps in the voltage magnitude data, as shown in the plot (a) of Fig. 6. The proposed approach detects all three *small* step changes in this case, as illustrated in Fig. 6(b). Note that the time-stamps are indicated in UTC time at PM.

These examples demonstrate that detecting step changes is crucial for analyzing the interactions between controllers involving IBRs and other devices. Studying these scenarios may justify the need for PV and OLTC control coordination to prevent unnecessary operation and maintenance costs, as suggested in [32].

C. Case 3: Event Detection

Event detection is a popular topic in the field, and it is known that typical outage events can result in step changes in the PMU data. We analyze the application of our detection method for a real-world outage event, shown in Fig. 7. This event is the result of a line outage occurring within a region where a 115-kV solar power plant and a switching substation are located. The proposed method was performed in sliding window with a window size of 3 seconds, using a total of 90 phasors in each moving window.

Figure 8 shows the detection performance of our approach in three consecutive moving windows. Although voltage fluctuations exist in windows 1 and 2 (please see (a) and (b) in

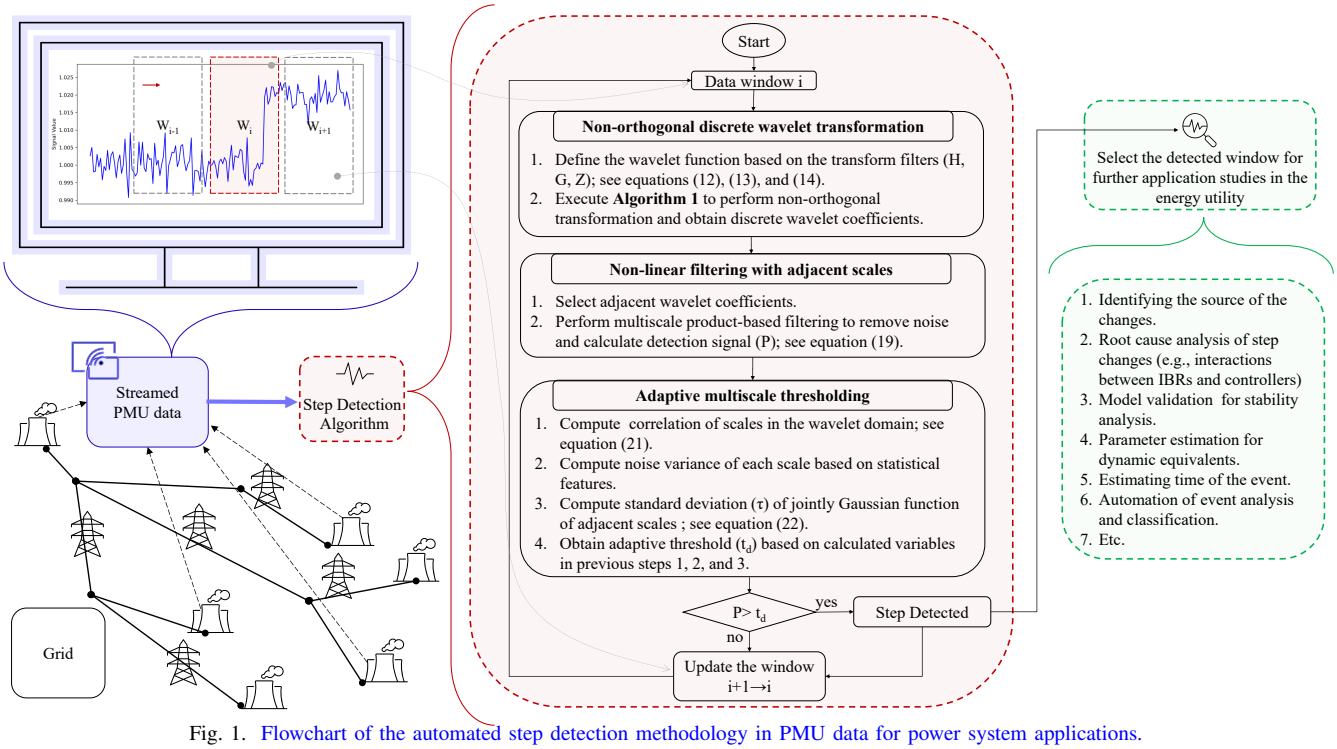

Fig. 1. Flowchart of the automated step detection methodology in PMU data for power system applications.

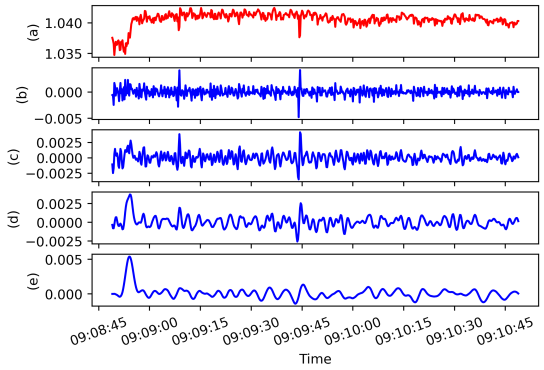

Fig. 2. An illustration of MZ-DWT, showing (a) the voltage time-series, and (b) to (e) the initial four scales of the DWT.

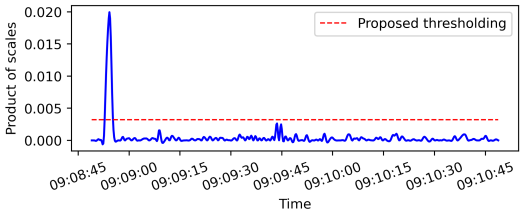

Fig. 3. The product of scales and the computed threshold for Case 1

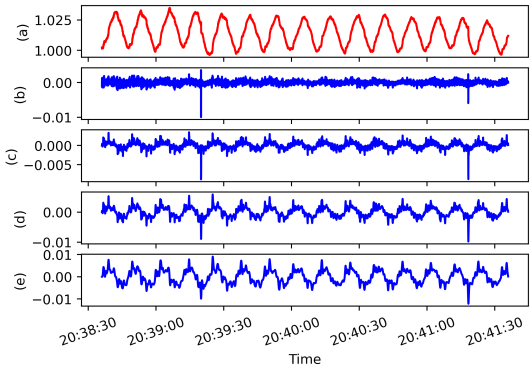

Fig. 4. An illustration of MZ-DWT, showing (a) the voltage time-series, and (b) to (e) the initial four scales of the DWT.

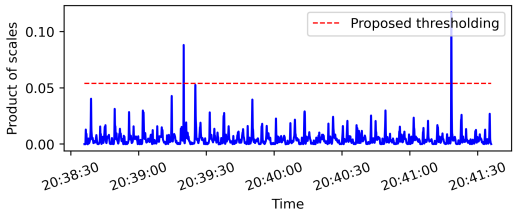

Fig. 5. The product of scales and the computed threshold for Case 2.

Fig. 8), the detection threshold, indicated by the red dotted line, does not give a false alarm. In the third window, the line outage occurs, creating a *unique response* with two-step changes which are detected precisely. In this window, the onset of the first step in PMU voltage data is associated with the occurrence of the line outage at 7.66 (= 6 + 1.66) seconds. The step change time within PMU data is computed as the instance corresponding to the maximum value observed in the multiscale filtered data $P_j g$. Consequently, precise estimation of the event time is indicated by $t = \arg\max(P_j g)$, which is equal to 1.66 seconds in the third window.

Detecting abrupt changes and their timing is crucial in power system studies such as inertia estimation, parameter identification, online monitoring, etc.

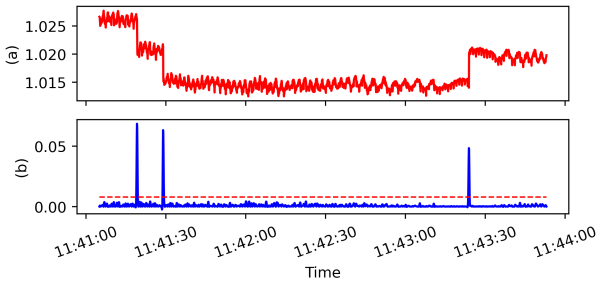

Fig. 6. The profiles of (a) measured voltage data and (b) scales multiplications and the computed threshold. Note: time-stamps are PM in UTC time.

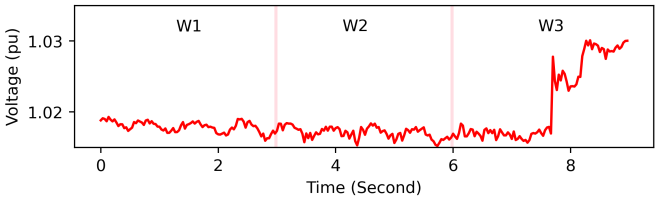

Fig. 7. Recorded voltage profile for Case 3 (Wi = Sliding window number i)

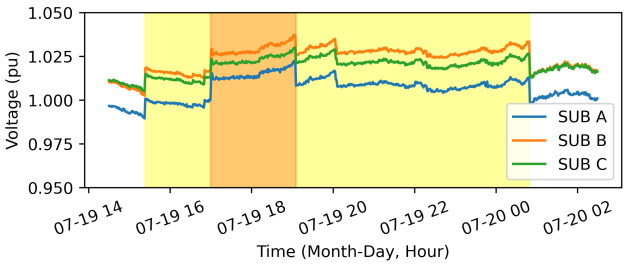

Fig. 9. The profiles of voltage in three real-world substation.

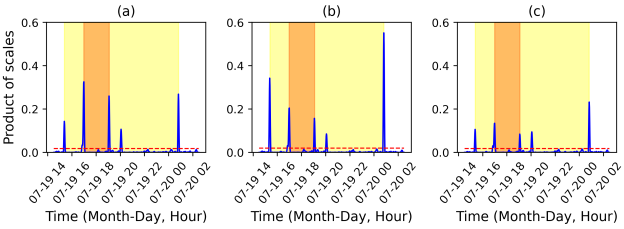

Fig. 10. The product of scales and the computed threshold (shown with dotted red lines) for three different locations: (a) Substation A, (b) Substation B, and (c) Substation C.

D. Case 4: Locating The Source of Step Changes

In this section, we consider preprocessed voltage measurements obtained over 12 hours from three PMUs located at three different 230-kV substations, shown in Fig. 9. The three substations, SUB A, B and C in Fig. 9, are interconnected through transmission lines. Furthermore, the capacitor banks installed at substations A and B are initially connected and subsequently disconnected. Their operation periods, which start with a switch-on and end with a switch-off, are highlighted in Fig. 9 (orange for A and yellow for B).The voltage steps (up and then down) during the operation of the capacitor banks are visible in the PMU data in Fig. 9.

The proposed method is applied to the three streams of PMU data at the different substations, and the results from nonlinear filtering with multiscale products are presented in Fig. 10. Our method effectively detects the step changes that we focus on in this application.

Let us concentrate on the period highlighted in orange in Fig. 10, during which the capacitor bank in substation A is connected at the beginning and disconnected at the end of this colored interval. As shown in Fig. 10(a), the magnitudes of the peaks in substation A are greater during this interval compared to the magnitudes in plots (b) and (c), which represent the voltage at substations B and C, respectively. This confirms the fact that the capacitor bank switching occurs at SUB A, as the voltage is affected by the injection of reactive power at the substation where it is measured. Now, our focus shifts to the period highlighted in yellow, where the capacitor bank of substation B is connected at the beginning and then disconnected at the end of this interval. As shown in Fig. 10(b), associated with SUB B, the multiscale filtered data reveal higher maxima (peaks) at the onset and end of this yellow-colored interval compared to other maxima shown in plots (a) and (c) for SUB A and SUB C within the same time interval.

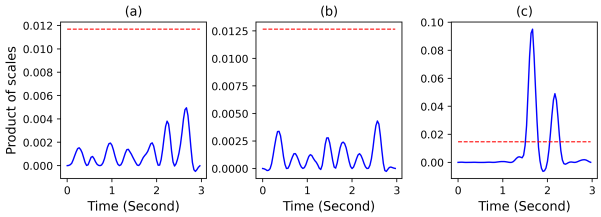

Fig. 8. The product of scales and the computed threshold (shown with dotted red lines) for three consecutive windows: (a) Window 1, (b) Window 2, and (c) Window 3

These findings demonstrate that the peaks of multiscale products are not only useful for detecting step changes but also can serve as a criterion for identifying the source of these changes. Identifying the location where the step change originates from and subsequently selecting the appropriate window of data from the available PMUs at different locations is useful for power system studies, such as computing Q-V sensitivities to assist in voltage stability analyses [33]. For illustration, we used two consecutive data windows from the bus in SUB A for Q-V sensitivity analysis. In the first window, the step change occurs due to an external source (grid-induced action), while in the second window, the step change occurs due to internal source (switching on of a capacitor bank) in SUB A, denoted as a locally-induced action. The sensitivities dV/dQ in windows 1 and 2 are computed for the bus in SUB A using the linear regression routine in *statsmodels* [34], yielding: - 0.012 and 0.049, respectively. The observed positive values can be attributed to the activation of the capacitor bank in SUB A, which raises the voltage magnitude and concurrently introduces extra reactive power. The systematic application of the proposed automated method along with the sensitivity computations can help utilities in planning studies, such as studying the sensitivity of a particular bus and finding impedance equivalents from the perspective of that bus, as shown in the examples in [35].

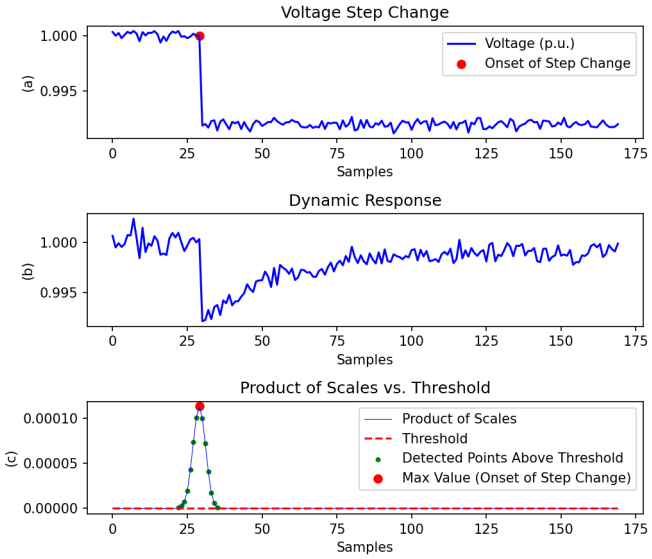

Fig. 11. The profile of (a) voltage magnitude before and after the step change, (b) outputted power under the dynamic response, and (c) the detection signal and thresholding.

IV. Further Applications

A. Supporting Parameter Estimation for Dynamic Equivalents

Dynamic equivalents can be used for stability analysis for a grid (or portion thereof) where a model is not available, or where a low-order simplified representation is needed. The equivalent model represents the whole or part of the actual power system, for which estimated parameters are needed. To automate this process for utilities, it is important to detect step changes in the data stream and locate its time of occurrence.

To illustrate part of this process, we consider a synthetic first-order dynamic response in [18] under 0.8% step change in the voltage signal, as shown in Fig. 11(a). Meanwhile, Fig. 11(b) shows the system's dynamic response under this step change. Applying the method proposed in this paper, the step change is detected accurately and its timing is located using our proposed method, as shown in Fig. 11(c).

Now, consider a scenario in which we have an extensive stream of data. The proposed method can effectively identify and select the appropriate windows where the step changes occur, facilitating dynamic response analysis. Furthermore, the proposed threshold can be used to separate noise from the underlying pattern, helping to reconstruct clean measured data without noise using the *inverse* of wavelet transformation. This can significantly improve data quality, a necessary task for the accurate identification of the parameters of the equivalent model [18].

B. Supporting Model Validation for Stability Analysis

Power system stability analysis requires accurate physics-based models. The model becomes inaccurate when there is a discrepancy between the assumed model and the actual measured response. Model validation is necessary to confirm the accuracy of the model and, consequently, that of the different stability analyses that use the model. One of the particular stability analysis methods of interest is small-signal

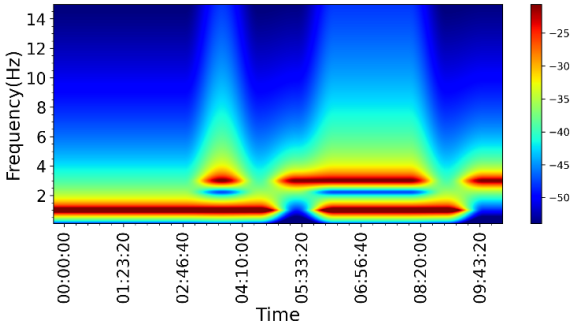

Fig. 12. The spectrogram of the system's actual response.

stability, where the system's dominant modes and mode-shapes are determined and stability margins are determined [36]. This stability analysis can alternatively be performed using PMU data [37]. Hence, a difference between the mode estimates vs. modes determined using a physics-based model can indicate potential inaccuracies in the physics-based model, as long as the mode estimates have been obtained with relatively low variance [38]. Hence, model validation w.r.t. small-signal analysis would imply comparing the error between the identified and computed modes modes, and could be performed based on different methods, such as residual-based analysis [39].

To illustrate, we consider a mode estimation algorithm based on the Yule-Walker method, which is established for a synthetic system with a 1 Hz mode [13]. We now evaluate the validity of a corresponding simulation model by examining its system response under ambient conditions, e.g., considering load or generation variations, controller responses, etc., and by using residual analysis. If the simulation model's response is valid, only small residuals close to zero should appear. Otherwise, larger residual values indicate a mismatch between the model and the actual system.

To perform this analysis, we produce two data sets, the "actual" system response, which includes unmodeled dynamics compared to the "simulation" model, illustrated in Fig. 12. This figure shows the spectrogram of our system's actual response with mode changes over time. Next, recall that our power system model includes only a 1 Hz mode. By visual inspection of Fig. 12, it can be observed that the actual response of the system contains two modes, while the simulation model contains only one mode. This implies that the simulation model is not accurate, as it does not model certain dynamics observed in the actual response. To quantify this, in Fig. 13(a), the residual changes due to the mismatch between the actual response of the system and the simulation model appear as step changes. Hence, the proposed step detection method can identify inaccuracies in the model as the system condition changes, as shown in Figure 13(b), making it suitable for testing the validity of the model.

Please note that the illustrations in the previous two sections are meant to discuss the *potential applications* of the proposed methodology for different types of studies. The applications in question require further development, which is *not* within the scope of this paper.

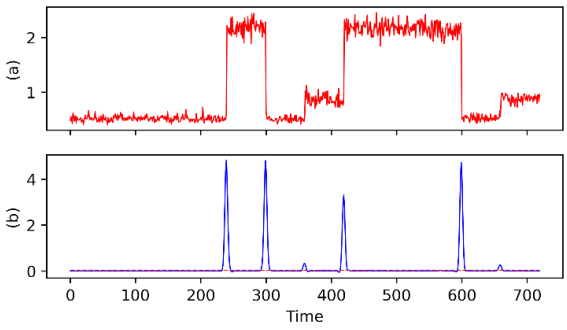

Fig. 13. The profile of (a) residuals, and (b) step detector.

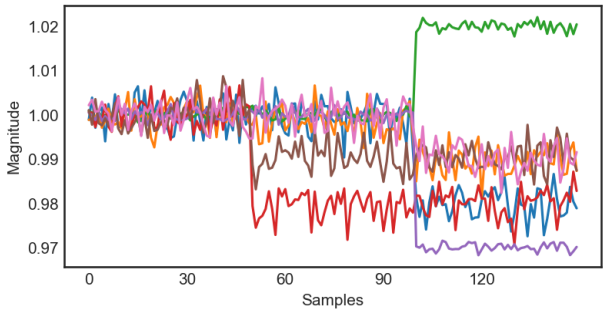

Fig. 14. Samples of generated scenarios with step changes. Each color corresponds to a different scenario.

V. Comparison of Methods

A. Quantitative Comparisons

In detection methods, there are two primary steps: first, the original signal is characterized and referred to as the detection signal, followed by setting a threshold for this detection signal. The effectiveness of this thresholding process is closely linked to the quality of the detection signal obtained.

We generate 100 scenarios that involve step changes and another 100 scenarios that represent normal operating conditions for detection analysis. Each synthetic PMU data stream is 5 seconds long and is "reported" at 30 phasors per second. Signal-to-noise ratio (SNR) values of 40, 50, and 60 are randomly added to the signal, creating realistic Gaussian noise. Moreover, small magnitude step changes, ranging from -3%, -2%, -1% to 1%, 2%, and 3% of the signal, are randomly applied to a signal with a magnitude of 1. Fig. 14 shows a few samples of the generated scenarios.

Using the prepared data set, different step detection approaches are compared as follows:

- The orthogonal db1 wavelet is used for signal characterization because it shows promising performance in power system studies that deal with abrupt change detection [15]. This choice is meaningful and intuitive because of the step-like pattern of the db1 or Haar wavelet. Our experiments show that the results of scale 3 and scale 4 of this transformation provide distinctive features as a detection signal to be used for step detection. Universal thresholding is used for these cases because it is effective and relevant for wavelet applications [40], [41].
- A gradient estimator employing an FIR filter configured as [-1, 0, 1] is used [21]. This is *not* based on wavelet theory. This approach is used effectively in edge/step detection problems. The threshold based on Median Absolute Deviation (MAD) [42], is used to detect steps.
- A *Hilbert-based detection* method proposed in [43] is adopted for comparison with the proposed method. The Hilbert-based method was used for step detection of signals in the context of phasor measurement unit calibration as described in [43].
- A *data-driven detection* method with multi-band features, as proposed in [44], [45], is selected for our comparisons. This was used for event detection problems and creates signal bands with statistical features to capture overshoots and undershoots in PMU data, as described in [44], [45].
- Our proposed gradient estimation-based *wavelet* is used to characterize the signal. The MAD-based threshold is set on a single wavelet scale. In another strategy, we use multiscale filtering of our proposed wavelet and then the proposed thresholding method on it, which is our best proposed solution for step detection.

We aim to detect steps (positive class) versus non-steps (negative class) and analyze the performance of the models using different metrics. ACC measures the proportion of correct detections (both steps and non-steps) out of the total number of cases. It is defined as:

$$\text{ACC} = \frac{TP + TN}{TP + TN + FP + FN} \tag{23}$$

where TP represents True Positives, which are correctly detected steps; TN indicates True Negatives, which are correctly identifying non-steps; FP is False Positives, incorrectly detecting steps; and FN represents False Negatives, which are undetected step changes. Moreover, precision (PRE) measures the proportion of correctly detected steps out of all cases detected as steps. It is defined as:

$$\text{PRE} = \frac{TP}{TP + FP} \tag{24}$$

The F1 score represents the harmonic mean of Precision and Recall, offering a balanced metric that is particularly valuable in scenarios where both false positives and false negatives are critical, such as in power system applications. This score is defined as:

$$\text{F1} = 2 \times \frac{\text{PRE} \times \text{Recall}}{\text{PRE} + \text{Recall}} \tag{25}$$

where Recall is expressed as $\frac{\text{TP}}{\text{TP+FN}}$. These metrics evaluate detection or classification performance by providing a quantitative measure ranging from 0 to 1 [46].

As indicated in Table I, our proposed method based on multiscale thresholding significantly outperforms others in different metrics across 200 scenarios. To visualize this assessment, we chose to show two scenarios with step changes, as illustrated in Fig. 15.(a) and Fig. 16.(a). The unsuccessful detection performance of the Hilbert-based technique [43] and the data-driven detection solution [44] are shown in Fig. 15.(b) and 16.(b), where the computed thresholds could not detect step changes.

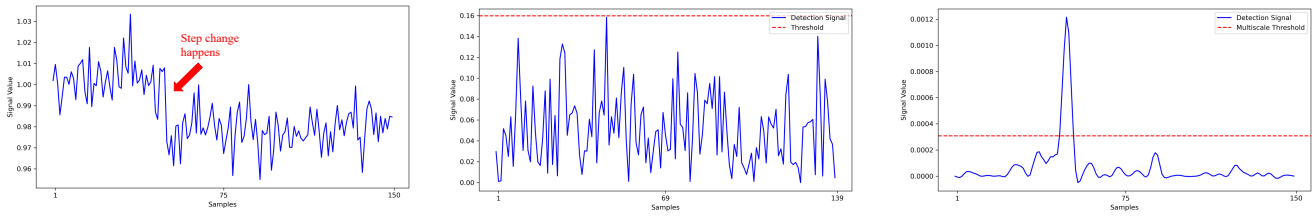

(a) (b) (c)

Fig. 15. Illustrative comparison with Hilbert-based method [43]: a) signal with step changes, b) Hilbert-based detection performance, c) proposed method's performance.

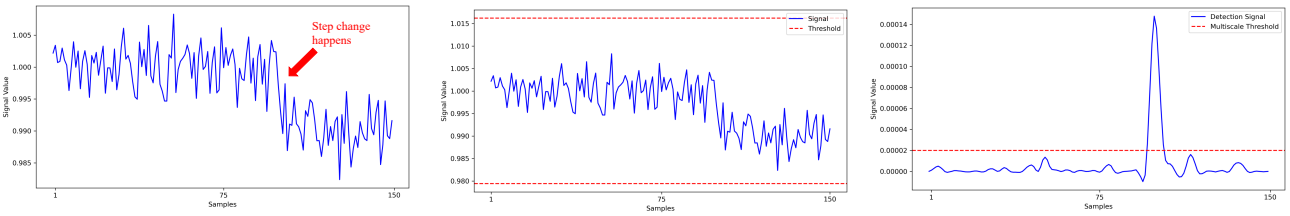

(a) (b) (c)

Fig. 16. Illustrative comparison with data-driven method [44]: a) signal with step changes, b) Data-driven detection performance, c) proposed method's performance.

Referring to Fig. 15.(b), observe that the Hilbert-based method shows high sensitivity to noise, causing false alarms under ambient data, which is also evident in the metric scores in Table I. Meanwhile, as it can be observed in Fig. 16.(b), the data-driven method establishes thresholds directly on the original data and creates overshoot and undershoot bands, which results in poor detection performance. In contrast, our proposed method first transform the data to obtain better signatures and then establishes the threshold on the new representation of the data.

Observe in Figs. 15.(c) and Figs. 16.(c) that our method is capable of recognizing the step changes as it established a threshold that can effectively detect them in both cases. This is thanks to the three-stage process where the data transform into a well-represented domain with nonorthogonal wavelets, the noise is suppressed efficiently with multiscale product filtering, and finally, computing a multiscale adaptive threshold based on the grid conditions and signal features.

It should be pointed out that the second-best performing method is also based on our proposed wavelet transformation, but implements a single-scale threshold. This results in performance degradation when compared with the proposed multiscale-based method, as evidenced by an 8.4% drop in PRE. Despite this, it still outperforms all baseline methods thanks to the effective data transformation with our suggested nonorthogonal wavelet method.

TABLE I
COMPARING THE PERFORMANCE OF STEP DETECTION APPROACHES

Detection Strategy	ACC %	F1 %	PRE %
Universal threshold with db-1 (scale 3)	0.680	0.712	0.648
Universal threshold with db-1 (scale 4)	0.610	0.675	0.579
Gradient estimation with FIR filter	0.735	0.749	0.712
Hilbert-based method	0.579	0.695	0.541
Data-driven detection method	0.625	0.640	0.614
Proposed wavelet with single-scale thresholding	0.865	0.874	0.817
Proposed wavelet with *multiscale* thresholding	**0.905**	**0.905**	**0.901**

B. Qualitative Comparisons

Our method presents several benefits, as detailed below:

1) Application Versatility: As shown in Sections II, the proposed method can be used for multiple applications such as effectively detecting capacitor bank switching, OLTC responses to IBR operations, line outages, and newly induced modes under oscillations. It also pinpoints the timing of these changes, which is crucial for automated utility studies, including model validation and parameter estimation. In contrast, the studies in [15] and [17] focus solely on detecting events that cause significant changes in the magnitudes of measured signals and do not demonstrate applications for ambient data analytics or the tracking of changes under ambient conditions.

2) Robustness to Ambient Noise: A challenge in working with real-world synchrophasor data is the effect of random load variations, which excite small-signal dynamics under normal conditions and are referred to as ambient data. Ambient data pose challenges in detection, such as the risk of false positives in detection applications (e.g. the Band 1 filter used to monitor WECC in BPA [47]). The proposed method demonstrates minimal sensitivity to noise and system dynamic changes by employing a highly robust threshold that is updated based on noise levels (see Table 1) and grid dynamical conditions (see Section III, Figures 7 and 8). This capability will be particularly beneficial in the future, given the increased integration of IBRs, data centers, and new components that influence system dynamics [5]. In contrast, other statistical and signal processing methods, such as MAD and universal thresholding [40], [45], often struggle to effectively distinguish noise features from the underlying desired patterns compared

to our method.

3) Adaptivity without Requiring Historical Data: The method does not require prior knowledge or historical data to establish a baseline to characterize normal behavior in detection. Instead, it relies solely on data from the monitored window, without requiring the complex task of setting parameters, and it adapts to evolving changes, making it highly practical, robust, and adaptive. Unlike conventional studies that require extensive baselining studies and training datasets [48], the proposed method can be effectively applied without the burden involved with existing and emerging methods [15], [16], [17], [49]. This is particularly important because, in practice, large datasets are not always well-organized, stored, or cleaned for analysis, and may not be applicable for the actual power grid of interest.

VI. Conclusions

This paper introduced a robust framework for detecting step changes in real-world PMU data. The operation of different power equipment frequently appears as steps in synchrophasor data, and accurately detecting and locating these steps can significantly help in selecting appropriate data windows for power system studies, understanding controller responses, detecting events or set point changes, conducting root cause analysis, and to support other analysis applications.

The proposed method was developed using the nonorthogonal wavelet transformation and smoothed gradient estimation. It was designed to characterize edges in signals at multiple scales using local maxima while preserving temporal information in all scales. Motivated by the Lipschitz regularity concept, multiscale product theory was then applied to effectively extract distinctive step-related features across scales while filtering out noise. Finally, the adaptive threshold on the multiscale filtered data completed the detection task in our automated step detection process.

The proposed approach was able to detect both small and large step changes in synchrophasor data effectively while providing information on the instant of the step changes. The method does not require historical data or learning datasets, making it practical for real-world problems. Furthermore, we illustrated how the method can support practical applications by showcasing various case studies.

References

[1] J. De La Ree, V. Centeno, J. S. Thorp, and A. G. Phadke, "Synchronized phasor measurement applications in power systems," *IEEE Trans. Smart Grid*, vol. 1, no. 1, pp. 20–27, 2010.

[2] Y. Cheng *et al*, "Real-world subsynchronous oscillation events in power grids with high penetrations of inverter-based resources," *IEEE Trans. on Power Syst.*, vol. 38, no. 1, pp. 316–330, 2023.

[3] M. Almas, M. Baudette, and L. Vanfretti, "Utilizing synchrophasor-based supplementary damping control signals in conventional generator excitation systems," *Electric Power Systems Research*, vol. 157, pp. 157–167, 2018.

[4] J. Lavenius, L. Vanfretti, and G. N. Taranto, "Performance assessment of pmu-based estimation methods of Thévenin equivalents for real-time voltage stability monitoring," in *2015 IEEE 15th Intl. Conf. on Environment and Electrical Eng. (EEEIC)*, 2015, pp. 1977–1982.

[5] C. Mishra, L. Vanfretti, J. Delaree, and K. D. Jones, "Analyzing a non-sinusoidal response from a real-world solar PV," *IEEE Trans. Power Syst.*, pp. 1–4, 2024.

[6] P. Wall and V. Terzija, "Simultaneous estimation of the time of disturbance and inertia in power systems," *IEEE Trans. Power Deliv.*, vol. 29, no. 4, pp. 2018–2031, 2014.

[7] M. Podlaski, L. Vanfretti, J. Pesente, and P. H. Galassi, "Automated parameter identification and calibration for the Itaipu power generation system using Modelica, FMI, and RaPId," in *2019 7th Workshop on MSCPES*, 2019, pp. 1–6.

[8] A. Raghami, G. Ledwich, Y. Mishra, and G. Walker, "Simultaneous local identification of Thévenin equivalent impedances in a distribution system," *IEEE Trans. Power Syst.*, pp. 1–9, 2023.

[9] D. Georgakopoulos and S. Quigg, "Precision measurement system for the calibration of phasor measurement units," *IEEE Trans. Instrum. Meas.*, vol. 66, no. 6, pp. 1441–1445, 2017.

[10] G. Frigo, D. Colangelo, A. Derviškadić, M. Pignati, C. Narduzzi, and M. Paolone, "Definition of accurate reference synchrophasors for static and dynamic characterization of pmus," *IEEE Trans. Instrum. Meas.*, vol. 66, no. 9, pp. 2233–2246, 2017.

[11] G. A. Kyriazis, W. G. Kürten Ihlenfeld, and R. P. Landim, "Estimating parameters of combined am and pm signals using prior information," *IEEE Trans. Instrum. Meas.*, vol. 64, no. 6, pp. 1760–1766, 2015.

[12] M. B. Martins, R. T. de Barros e Vasconcellos, and P. A. A. Esquef, "Step change detection based on analytic signal for pmu calibrators," in *2019 IEEE 10th AMPS*, 2019, pp. 1–5.

[13] C. Wang *et al*, "Identifying oscillations injected by inverter-based solar energy sources," in *2022 IEEE PESGM*, 2022, pp. 1–5.

[14] X. Xu *et al*, "Tracking periodic voltage sags via synchrophasor data in a geographically bounded service territory," in *2023 IEEE PES Grid Edge*, 2023, pp. 1–5.

[15] D.-I. Kim *et al*, "Wavelet-based event detection method using pmu data," *IEEE Trans. Smart Grid*, vol. 8, no. 3, pp. 1154–1162, 2017.

[16] Y. Liu *et al*, "Robust event classification using imperfect real-world PMU data," *IEEE Internet of Things Journal*, 2022.

[17] A. Ghasemkhani, Y. Liu, and L. Yang, "Real-time event detection using rank signatures of real-world pmu data," in *2022 IEEE Power Energy Society General Meeting (PESGM)*, 2022, pp. 1–5.

[18] E. P. Saroudis *et al*, "Automatic processing of dynamic responses via wavelet transform for the development of dynamic equivalent models," *Sustainable Energy, Grids and Networks*, vol. 38, p. 101383, 2024.

[19] S. Mallat and S. Zhong, "Characterization of signals from multiscale edges," *IEEE Trans. Pattern Anal. Mach. Intell.*, vol. 14, no. 7, pp. 710–732, 1992.

[20] A. Rosenfeld, "A nonlinear edge detection technique," *Proceedings of the IEEE*, vol. 58, no. 5, pp. 814–816, 1970.

[21] B. Sadler and A. Swami, "Analysis of multiscale products for step detection and estimation," *IEEE Trans. Inf. Theory*, vol. 45, no. 3, pp. 1043–1051, 1999.

[22] M. M. Lakouraj, C. Mishra, J. De La Ree, L. Vanfretti, K. D. Jones, and H. Livani, "Detection of step changes in real-world synchrophasor measurements," in *2024 IEEE Power Energy Society General Meeting (PESGM)*, 2024, pp. 1–5.

[23] J. Canny, "A computational approach to edge detection," *IEEE Trans. Pattern Anal. Mach. Intell.*, vol. PAMI-8, no. 6, pp. 679–698, 1986.

[24] P. Bao and L. Zhang, "Noise reduction for magnetic resonance images via adaptive multiscale products thresholding," *IEEE Trans. Med. Imag.*, vol. 22, no. 9, pp. 1089–1099, 2003.

[25] S. Mallat, "Multifrequency channel decompositions of images and wavelet models," *IEEE Transactions on Acoustics, Speech, and Signal Processing*, vol. 37, no. 12, pp. 2091–2110, 1989.

[26] S. Mallat and W. Hwang, "Singularity detection and processing with wavelets," *IEEE Trans. Inf. Theory*, vol. 38, no. 2, pp. 617–643, 1992.

[27] L. Zhang and P. Bao, "Edge detection by scale multiplication in wavelet domain," *Pattern Recognition Letters*, vol. 23, no. 14, pp. 1771–1784, 2002.

[28] P. Bao, L. Zhang, and X. Wu, "Canny edge detection enhancement by scale multiplication," *IEEE Trans. Pattern Anal. Mach. Intell.*, vol. 27, no. 9, pp. 1485–1490, 2005.

[29] D. L. Donoho and I. M. Johnstone, "Ideal spatial adaptation by wavelet shrinkage," *biometrika*, vol. 81, no. 3, pp. 425–455, 1994.

[30] P. Castello, C. Muscas, and P. A. Pegoraro, "Statistical behavior of pmu measurement errors: An experimental characterization," *IEEE Open Journal of Instrumentation and Measurement*, vol. 1, pp. 1–9, 2022.

[31] M. Brown *et al*, "Characterizing and quantifying noise in PMU data," in *2016 IEEE PESGM*, 2016, pp. 1–5.

[32] P. R. D. Monteiro, L. P. Gama, T. T. Borges, M. Z. Fortes, and L. F. Henrique, "Impact on on-load tap-changer transformers in industries due to high penetration of photovoltaic distributed generation," *Electrical Engineering*, pp. 1–11, 2024.

[33] R. Leelaruji *et al*, "Computing sensitivities from synchrophasor data for voltage stability monitoring and visualization," *International Transactions on Electrical Energy Systems*, vol. 25, no. 6, pp. 933–947, 2015. [Online]. Available: https://onlinelibrary.wiley.com/doi/abs/10.1002/etep.1869

[34] S. Seabold and J. Perktold, "statsmodels: Econometric and statistical modeling with python," in *9th Python in Science Conference*, 2010.

[35] C. Mishra *et al*, "Designing model-free time derivatives in the frequency domain for ambient PMU data applications," in *2022 IEEE PESGM*, 2022, pp. 1–5.

[36] N. Martins, P. E. Quintão, H. Pinto, A. de Castro, S. Gomes Jr, and J. C. Ferraz, "A small-signal stability program incorporating advanced graphical user interface," *Proceedings of the VII SEPOPE*, 2000.

[37] L. Vanfretti *et al*, "Application of ambient analysis techniques for the estimation of electromechanical oscillations from measured pmu data in four different power systems," *European Transactions on Electrical Power*, vol. 21, no. 4, pp. 1640–1656, 2011.

[38] S. B. *et al*, "Probing signal design for enhanced damping estimation in power networks," *International Journal of Electrical Power Energy Systems*, vol. 129, p. 106640, 2021.

[39] Z. Cao and J. W. Pierre, "Electromechanical mode estimation validation using recursive residual whiteness testing," in *2013 North American Power Symposium*, 2013, pp. 1–6.

[40] M.-H. Wang, S.-D. Lu, and R.-M. Liao, "Fault diagnosis for power cables based on convolutional neural network with chaotic system and discrete wavelet transform," *IEEE Trans. Power Deliv.*, vol. 37, no. 1, pp. 582–590, 2022.

[41] A. Ukil and R. ivanovi, "Application of abrupt change detection in power systems disturbance analysis and relay performance monitoring," *IEEE Trans. Power Deliv.*, vol. 22, no. 1, pp. 59–66, 2007.

[42] C. Leys *et al*, "Detecting outliers: Do not use standard deviation around the mean, use absolute deviation around the median," *Journal of experimental social psychology*, vol. 49, no. 4, pp. 764–766, 2013.

[43] M. B. Martins, R. T. de Barros e Vasconcellos, and P. A. A. Esquef, "Models for synchrophasor with step discontinuities in magnitude and phase: Estimation and performance," *IEEE Transactions on Instrumentation and Measurement*, vol. 68, no. 6, pp. 2007–2014, 2019.

[44] A. Shahsavari *et al*, "Situational awareness in distribution grid using micro-PMU data: A machine learning approach," *IEEE Trans. Smart Grid*, vol. 10, no. 6, pp. 6167–6177, 2019.

[45] M. Naglic *et al*, "Synchronized measurement technology supported AC and HVDC online disturbance detection," *Electric Power Systems Research*, vol. 160, pp. 308–317, 2018.

[46] M. Grandini, E. Bagli, and G. Visani, "Metrics for multi-class classification: an overview," *arXiv preprint arXiv:2008.05756*, 2020.

[47] D. Kosterev et al., "Implementation and operating experience with oscillation detection application at bonneville power administration," in *Proceedings of CIGRE 2016 Grid of the Future Conference*, 2016.

[48] P. Etingov, J. Follum, S. Biswas, and T. Yin, "Open source synergy: Developing and validating pmu data analysis techniques using open source tools and datasets," in *2024 International Conference on Smart Grid Synchronized Measurements and Analytics (SGSMA)*, 2024, pp. 1–6.

[49] T. Mohamed, M. Kezunovic, Z. Obradovic, Y. Hu, and Z. Cheng, "Application of machine learning to oscillation detection using pmu data based on prony analysis," in *2022 IEEE PES Innovative Smart Grid Technologies Conference Europe (ISGT-Europe)*, 2022, pp. 1–5.